OPEN ACCESS

University of BRISTOL

Wang, X. D., Robertson, P. A., Cascarini, F. J. J., Quinn, M. S., McManus, J. W., & Orr-Ewing, A. J. (2019). Observation of Rainbows in the Rotationally Inelastic Scattering of NO with CH4. *Journal of Physical Chemistry A*, *123*(36), 7758-7767. https://doi.org/10.1021/acs.jpca.9b06806

Peer reviewed version

Link to published version (if available):
10.1021/acs.jpca.9b06806

Link to publication record in Explore Bristol Research
PDF-document

This is the author accepted manuscript (AAM). The final published version (version of record) is available online via American Chemical Society at https://pubs.acs.org/doi/abs/10.1021/acs.jpca.9b06806 . Please refer to any applicable terms of use of the publisher.

University of Bristol - Explore Bristol Research
General rights

This document is made available in accordance with publisher policies. Please cite only the published version using the reference above. Full terms of use are available:
http://www.bristol.ac.uk/red/research-policy/pure/user-guides/ebr-terms/

Observation of Rainbows in the Rotationally Inelastic Scattering of NO with CH_4

Xu-Dong Wang†, Patrick A. Robertson†, Frederick J. J. Cascarini, Mitchell S. Quinn, Joseph W. McManus, and Andrew J. Orr-Ewing*

School of Chemistry, University of Bristol, Cantock's Close, Bristol, BS8 1TS, UK

* Author for correspondence. E-mail: a.orr-ewing@bristol.ac.uk

† These authors contributed equally to this work.

Abstract

Using a combination of velocity-map imaging and resonance-enhanced multi-photon ionization detection with crossed molecular beam scattering, the dynamics of rotational energy transfer have been examined for NO in collisions with CH_4 at a mean collision energy of 700 cm^{-1}. The images of NO scattered into individual rotational (j'_{NO}) and spin-orbit (Ω) levels typically exhibit a single broad maximum that gradually shifts from the forward to the backward scattering direction with increasing rotational excitation (i.e. larger Δj_{NO}). The rotational rainbow angles calculated with a two-dimensional hard ellipse model show reasonable agreement with the observed angles corresponding to the maxima in the differential cross sections extracted from the images for higher Δj_{NO} transitions, but there are clear discrepancies for lower Δj_{NO} (in particular, final rotational levels with j'_{NO} =7.5 and 8.5). The sharply forward scattered angular distributions for these lower Δj_{NO} transitions better agree with the predictions of an L-type rainbow model. The more highly rotationally excited NO appears to coincide with low rotational excitation of the co-product CH_4, indicating a degree of rotational product-pair anti-correlation in this bimolecular scattering.

1. INTRODUCTION

Rotational energy transfer (RET) is a facile and ubiquitous molecular process in important gas phase environments, such as flames, planetary atmospheres, and the interstellar medium.[1] The dynamics of RET have therefore been extensively studied both experimentally and theoretically, [2, 3] with crossed molecular beam (CMB) scattering experiments providing a direct means to examine RET mechanisms. In combination with resonance-enhanced multi-photon ionization (REMPI) and velocity-map imaging (VMI) detection methods, CMB experiments can be used to obtain the differential cross section (DCS) for the inelastic scattering with quantum-state resolution. Using these state-of-the-art experimental methods, numerous systematic investigations have reported the collisions of NO with rare gases, as well as of CO with He and Ne, and OH with He and Ar.[4-10]

In contrast, DCS measurements for collisions between two molecules remain largely unexplored.[11-18] This is probably because of the experimental and theoretical challenges introduced by the additional complexity of molecule-molecule collisions, both in molecular-beam preparation of the colliders, and in the analysis and interpretation of the results of experiments. For example, theoretical development of accurate multi-dimensional potential energy surfaces (PES) and computational simulation of the quantum scattering become much more challenging than for atom-diatomic molecule collisions. Furthermore, the open-shell nature of NO + CH_4 introduces additional problems associated with diabatization of the potentials.[19] Since many of the systems of practical interest in combustion and atmospheric chemistry involve molecule-molecule collisions, there is a strong desire to improve our understanding and modeling of the associated energy and angular momentum transfer. While there are pioneering reports of measurement of DCSs for molecule-molecule rotational energy transfer using CMB methods with rotatable detectors, with either universal mass-spectrometric or REMPI detection,[20-23] only very recently have some studies appeared which exploit the CMB-VMI approach. Examples include HCl colliding with N_2 or CH_4, where clear evidence of positive rotation-rotation correlations was observed,[24] as well as the first measurements of DCSs for diatomic/polyatomic molecule + diatomic molecule collisions, namely, NO + H_2 and D_2, ND_3 + H_2, and CH_3 + H_2, D_2 and N_2.[11, 12, 25, 26] Here, we focus on the rotationally

inelastic scattering of NO with CH_4. Although both NO and CH_4 molecules play significant roles in the chemistry of gaseous environments including planetary atmospheres and combustion systems, their inelastic collision dynamics have not been the subject of prior experimental or theoretical study.

The degree of rotational energy transfer between two colliding molecules is controlled by the intermolecular PES. As most inelastic collisions are dominated by repulsive interactions, it is possible to observe rotational rainbows, which are sensitive probes of the PES anisotropy.[27-30] Rotational rainbows manifest as angular maxima in the differential cross sections and have been observed in the elastic, rotationally inelastic, and reactive collisions of atoms and molecules.[31, 32] Simplified, but powerful, classical treatments based on model representations of the forms of the repulsive potentials, such as the two-dimensional hard ellipse model, can provide valuable understanding of the dynamics of the inelastic scattering.[33, 34] Furthermore, the lessons learned about rotational rainbows in the scattering of molecules with atomic species such as the rare gases can be applied to more complicated system with many more degrees of freedom.[31, 35-38] By contrast, L-type rainbows arise from attractive forces between collision partners.[9, 34, 36, 39, 40] Quantum mechanically, the L-type rainbows originate from partial waves with higher total angular momentum (J) than the glory partial wave, and can therefore only occur when these high partial waves contribute to the scattering cross-section. As these partial waves cannot transfer sufficient energy to excite a molecule to high rotational levels, L-type rainbows are particularly prominent for small changes in the rotational angular momentum (j) of the colliding molecule.[41] The inelastic scattering of NO with CH_4 provides an opportunity to observe these L-type rainbows by obtaining velocity map images for NO scattered into low final angular momentum states j'_{NO} (i.e. low Δj_{NO} transitions).

We report here a study of the rotationally inelastic scattering of NO with CH_4 at a mean collision energy of 700 cm^{-1}. DCSs for collisions of NO with CH_4 were experimentally measured using CMB methods coupled with j'_{NO}-level and spin-orbit state specific REMPI detection and VMI of the scattered NO. We apply the two-dimensional hard ellipse and L-type models to interpret the physical origins of the scattering-angle dependent structures that are observed in the DCSs.

2. EXPERIMENTAL METHODS

DCSs were measured using a newly developed crossed molecular beam apparatus with REMPI detection of the scattered products combined with velocity map imaging, as shown schematically in Figure 1. The apparatus was designed to be adaptable, allowing convenient interchange between parallel, crossed (90°) and counterpropagating (180°) molecular beam configurations, for inelastic and reactive scattering experiments. The chamber can also accommodate the generation of radical reactants using laser photolysis during the initial stages of a supersonic expansion. Specific details pertaining to this experiment are provided below.

Molecular beams were formed by supersonic expansion of gaseous samples through two pulsed valves (nozzle diameter 1 mm, General Valve Series 9) and were collimated by skimmers of 1 mm diameter (model 1, Beam Dynamics). A 2.5% gaseous mixture of nitric oxide (CK Special Gases Limited, 99%) in argon (Air Liquide, 99.8%) crossed a neat methane (Air Liquide, 99.5%) beam at a 90° angle. The stagnation pressure behind the pulsed nozzle for the expansion of both colliding partners was around 3 bar. In contrast to conventional CMB apparatuses with two separate differentially pumped source chambers, our design combines the required differential pumping for both molecular beams. A cylindrical sheath was used to isolate the scattering chamber from the source chamber, and the two chambers were separately evacuated by a series of turbomolecular pumps. A more detailed picture of the apparatus is given in supplementary Figure S1. A typical base pressure for the scattering chamber was 3×10^{-8} mbar with the pulsed valves closed, and $\sim10^{-6}$ mbar with the valves operating at 10 Hz.

UV radiation in the wavelength range 225-226 nm required for (1+1) REMPI detection of scattered NO was generated by frequency doubling in a BBO crystal the output of a tunable pulsed dye laser (Sirah, Model PRSC-G-24, using Coumarin 460 dye) pumped by a Nd:YAG laser (Quanta Ray GCR 200) operating at 10 Hz. Note that the blurring effect on the scattering images of the ion-recoil speed (around 14 m/s) introduced in the (1+1) REMPI detection scheme for NO is small compared to the energy resolution of our apparatus. The energy and linewidth of the probe laser beam were

1.0 mJ/pulse and 0.4 cm^{-1}, respectively and the beam was loosely focused into the ionization region of the scattering chamber with a 50-cm focal length lens. The distributions of population over NO rotational levels in the incident supersonic NO/Ar molecular beam, and in the inelastically scattered NO final levels, were probed using (1+1) REMPI spectroscopy through the (0, 0) band of the NO $A^2\Sigma^+ - X^2\Pi$ transition at wavelengths around 226 nm. To probe the rotational states j'_{NO} = 7.5, 8.5, 10.5, 11.5, 12.5, 13.5, 16.5, and 18.5 of NO ($X^2\Pi_{1/2}$), the R_{21} branch was used. For j'_{NO} =10.5, the overlapping Q_{21} + R_1 branch transitions were also used. These transitions via R_{21} branches probe the Λ−doublet state of f parity for all rotational levels. However, the transitions via the overlapping Q_{21}+R_1 branches probe the Λ−doublet state of e parity for j'_{NO} = 10.5. All spectral assignments were made using the PGOPHER program.[42] In our experiments, the Doppler shift of inelastically scattered NO is smaller than the laser linewidth, and therefore the laser frequency was fixed, rather than scanned over the full width of the Doppler profile of the transition(s).

Nitric oxide ions were extracted through the ion optics assembly, set for velocity map imaging conditions, and accelerated onto a position-sensitive detector consisting of a pair of microchannel plates (MCPs; 75-mm diameter), a phosphor screen and CCD camera. A high-voltage pulse with a width of about 100 ns was applied to the front microchannel plate to detect selectively a central portion of the ion packet. This pulse also acted as a mass gate to remove interferences from other ions. Since the temporal widths of the scattered NO product Newton spheres are around 150 ns in the experiments, the Finite Slice Analysis (FINA) method was used to reconstruct the images to obtain the velocity distributions of the scattered products.[43] After reconstruction, the images and the total translational energy distributions were sharper, but the overall profiles and peak positions remained similar. A more detailed discussion is given in the Supplementary Material. The two molecular beams and the REMPI probe laser beam propagated in a plane parallel to the face of the VMI detector, and were aligned to optimize the scattering signal. The nozzle producing the beam of neat methane was operated in a repeating mode of 50 shots on and 50 shots off. The desired scattering signal was then obtained by subtraction of the background (i.e. without methane) image from the total image.

The collision energy in the measurements was 700 ± 80 cm^{-1}, and was precisely determined by

analyzing velocity map images of the beam spots obtained using REMPI detection of NO present in the NO/Ar molecular beam, and seeded at low concentration into the CH_4 molecular beam. The measured mean collision energy agrees with a value of 680 cm^{-1} expected for molecular beam velocities of room temperature NO seeded in Ar, and of neat CH_4, of 560 and 1100 m/s, respectively.[44] The rotational level population distribution in the incident NO beam was determined by comparison of experimental spectra using an unfocused and attenuated ionization laser (with energy of less than 0.1 mJ per pulse to avoid saturation effects), with spectra simulated using the PGOPHER program. The NO molecules were determined to be cooled to a rotational temperature of 6 ± 2 K, at which 90% of NO molecules were in the lowest quantum state (j_{NO}=0.5, Ω=1/2) with equal population of the two Λ−doublet (e/f) levels. Supersonic expansion of neat CH_4 without a seed gas does not lead to comparably efficient rotational cooling. Previous investigation showed that after such an expansion, 31 % of the methane molecules were in j_{CH4}=0, 56% in j_{CH4}=1 and 13% in j_{CH4}=2.[45] In addition, it has been reported that the rotational temperature of CH_4 molecules in a neat methane molecular beam was estimated to be about 9 K from the measured speed distribution.[32, 46]

Because of the crossing timescale of several microseconds in the intersection region of the two molecular beams, the detection efficiency of the scattered products depended on their speeds in the laboratory frame. In order to correct for this non-uniform detection sensitivity, we employed a modification of the computer program simulation method of Liu[47] to apply a density-to-flux transformation. Further details of the procedure can be found in the Supplementary Material. We also studied the rotationally inelastic scattering of NO with Ar at a collision energy of 640 ± 65 cm^{-1} to compare the performance of the new apparatus to previously published studies, and for the purpose of comparison of the scattering dynamics with those for NO with CH_4.

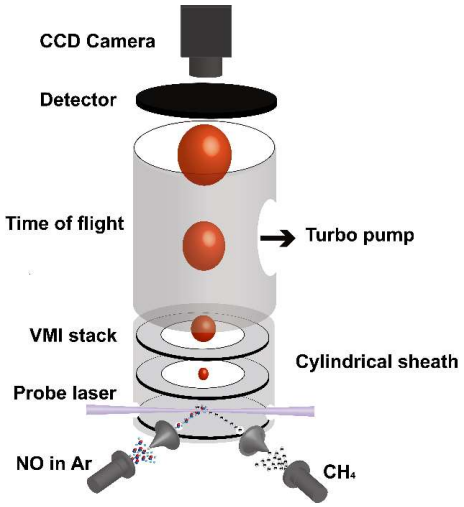

Fig. 1. Schematic diagram of the crossed molecular beam and velocity map imaging apparatus. The molecular beams crossed at 90° and the scattered products were detected by a UV laser beam with wavelengths tunable around 226 nm, focused at the center of the VMI ion optics by a 50-cm focal length quartz lens. The nascent NO^+ image was mass selected by time-of-flight and projected onto a two-dimensional imaging detector and then its position of impact recorded by a CCD camera.

3. RESULTS AND DISCUSSION

3.1 DCSs for rotationally inelastic scattering of NO with CH_4

The experimental velocity images for the inelastic scattering of NO with molecular methane, denoted by their respective final angular momentum quantum numbers j'_{NO}, are shown in Figure 2 for spin-orbit conserving ($\Omega = 1/2$) transitions into the final f Λ−doublet component of NO, CH_4 + NO ($^2\Pi_{1/2}$, j_{NO}=0.5, f/e) →CH_4 + NO ($^2\Pi_{1/2}$, j'_{NO}, f). The mean collision energy for this inelastic scattering is 700 cm^{-1}. At the same collision energy, spin-orbit changing transitions (to $\Omega = 3/2$) can also occur, and three images for lower Δj_{NO} transitions are given in Supplementary Figure S9. Images in Figure 2 are corrected with the density-to-flux transformation, and a Newton diagram is superimposed in the first panel. Any remaining asymmetry in the two halves of each image, separated by the relative velocity vector may be a consequence of an imperfect density to flux transformation, or fluctuations in factors such as laser intensity and molecular beam density. The center-of-mass (CM) frame scattering angle θ is defined as the angle between the CM-frame velocities of NO before and after a collision. It is clear from the images that the angular scattering distribution gradually shifts from the forward to the backward direction with increment of the final rotational energy of the scattered NO, behavior which is similar to that observed in the collision of

NO with Ar.[48] The character of the angular scattering distributions is almost the same for scattering into final levels of e and f parity. For example, detailed comparisons of images and DCSs of (j'_{NO}=10.5, f) and (j'_{NO}=10.5, e) are described in supplementary Figures S6, S7. The radius of the scattering sphere, which scales with the kinetic energy of the scattered products, decreases with increasing product rotational energy because of conservation of the total energy.

Imperfect subtraction of background signals arising from the unscattered and incompletely cooled NO molecules in the parent molecule beam (referred to here as a beam spot) means that the scattered products cannot be observed in the parts of images closest to the forward scattering direction. In some cases such as for j'_{NO} = 7.5, the forward scattering cannot be resolved on the right side of the image, but can be largely distinguished from the beam spot on the left side.

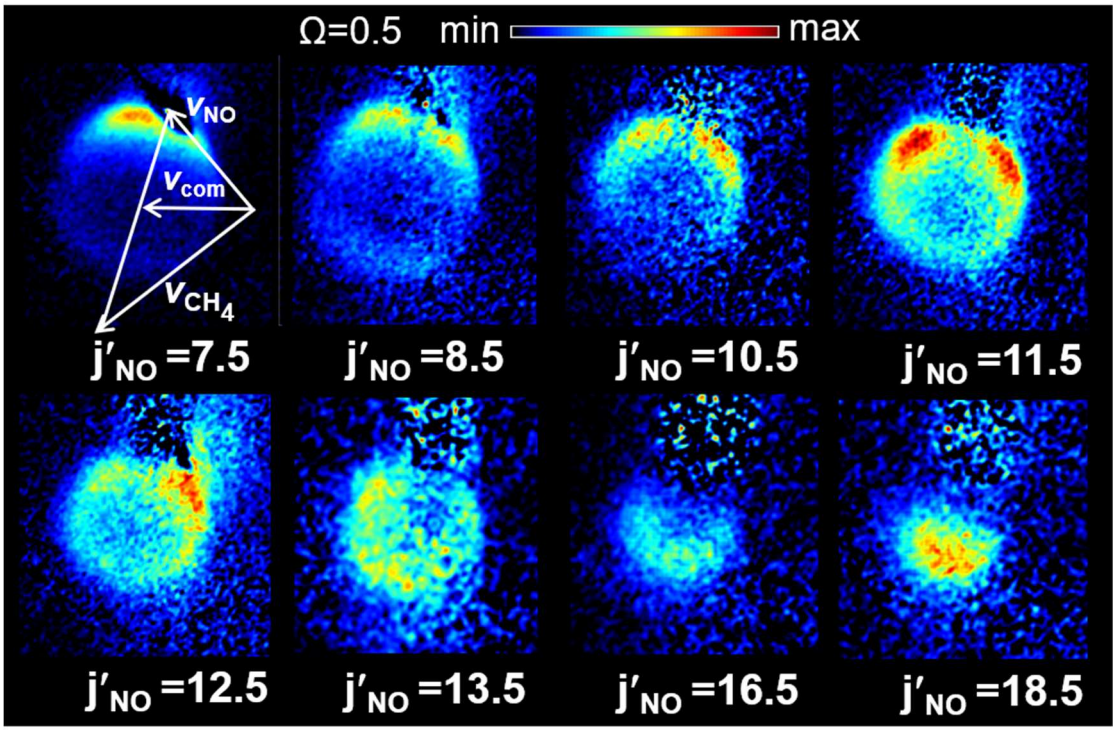

Fig. 2. Images for the inelastic scattering of NO with CH_4 into the final rotational levels of NO labelled. Images were obtained at a mean collision energy of 700 cm^{-1}. A Newton diagram superimposed in the top left panel shows the molecular beam velocities $\mathbf{v}_{NO}$ and $\mathbf{v}_{CH4}$, the center-of-mass velocity vector $\mathbf{v}_{com}$, and the relative velocity vector.

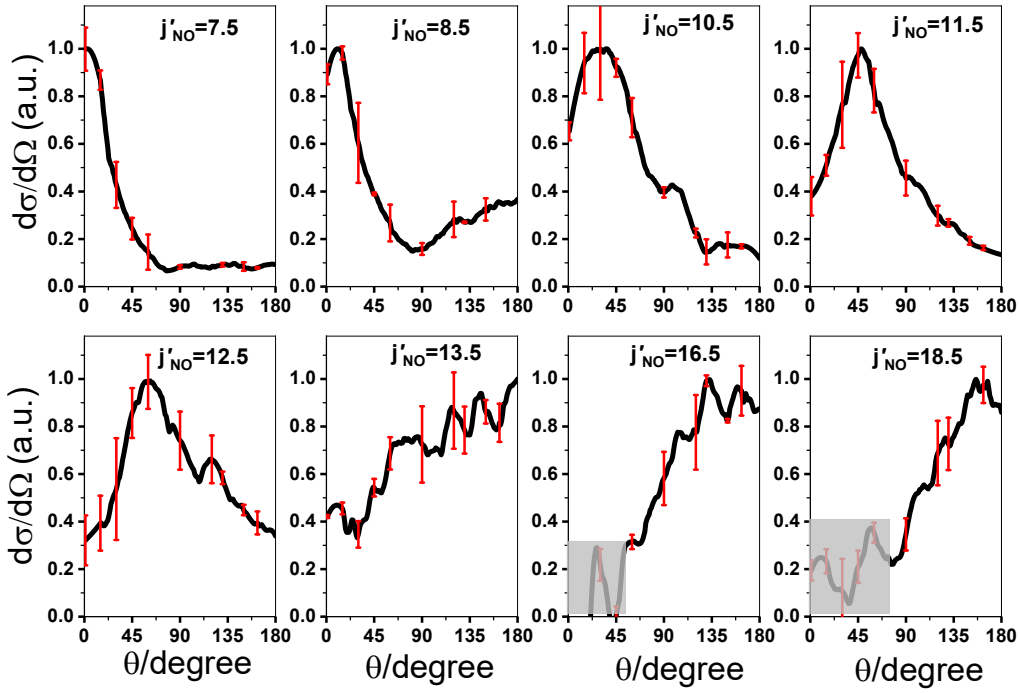

Fig. 3. Differential cross sections for the inelastic scattering of NO with CH_4 extracted from the experimental images shown in Figure 2. Labels on the panels indicate the final rotational levels of NO probe (all of parity). The error bars represent the intensity variation at the same scattering angle in the two halves of each image either side of the relative velocity vector. Small sections of the DCSs in the forward scattering direction are masked because, although the beam spots are weak at high j'_{NO}, so too are the forward scattered signals.

Figure 3 shows the DCSs (denoted as $d\sigma/d\Omega$ where Ω is the center-of-mass frame solid angle) for scattering into all experimentally measured NO final rotational levels, obtained by extracting angular product distributions from our images using a custom-written program based on the method of Hall and co-workers.[49] The experimentally recovered DCS has an arbitrary intensity based on the intensity of the experimental image, and therefore angular distributions normalized by maximum height are plotted. The trends observed in the DCSs confirm the qualitative conclusions drawn from the experimental velocity images: forward scattering is predominant for scattering into the lowest j'_{NO} states, with increasing sideways and backwards scattering observed for higher j'_{NO}. A single broad maximum in the images corresponding to a peak in the scattering intensity (suggesting a rotational rainbow) monotonically moves from forward to backward scattering with increasing Δj_{NO}, which is broadly consistent with scattering dynamics controlled by repulsive intermolecular interactions.

Similar behavior was previously observed for NO + rare gases inelastic scattering, and can be accounted for using a two-dimensional hard ellipse model.[38, 48, 50, 51] For NO + Ar inelastic scattering, two rotational rainbows corresponding to scattering at the N and O sites of NO were previously reported for j'_{NO} = 7.5 and 8.5.[48] To compare with the experiment results for inelastic scattering of NO with CH_4, rotationally inelastic scattering of NO with Ar, i.e., Ar + NO ($^2\Pi_{1/2}$, j_{NO}=0.5, f/e) →Ar + NO ($^2\Pi_{1/2}$, j'_{NO}, f), has been investigated at a collision energy of 640 ± 60 cm^{-1} using our apparatus. The newly measured images shown in Figure 4 agree well with the previous study by Yonekura *et al.*, and the positions of single or multiple rainbow peaks shown in Supplementary Figure S8 are also in quantitative agreement.[48] As shown in Figure 4, two rotational rainbows can be seen in both images of j'_{NO} = 7.5 and 8.5 in the NO + Ar system. Similarly, for NO + CH_4 inelastic scattering, images of j'_{NO} = 7.5 and 8.5 exhibit a broad distribution in the forward scattering direction and a minor distribution in the backward scattering direction (see Figure 2). Considering the similar character, small differences in collision energy and the velocity and angular spreads for the molecular beams inferred from the analysis of NO beam spots measured by VMI, it is possible that rotational rainbows are also observed in the NO + CH_4 inelastic scattering. Apart from the main character of a single broad maximum in the DCSs, some oscillatory structures can be seen, in particular for the higher final rotational levels (j'_{NO} =13.5, 16.5). Considering the spread in the collision energy (on the order of 10%) and the angular resolution of images (5° – 13°), the oscillatory structures in our DCS plots are more likely to be associated with experimental noise than quantum mechanical effects.

Our images for inelastic scattering of NO with CH_4, including those processed by the reconstruction software FINA (see Figure S4) display obviously broader distributions in the radial (speed) coordinate than is the case for Ar scattering with NO. These broad distributions indicate rotational excitation of the co-product CH_4, which is discussed further in section 3.3. However, the general behavior of the two systems, with a shift from forward to backward scattering as Δj_{NO} increases, is strikingly similar.

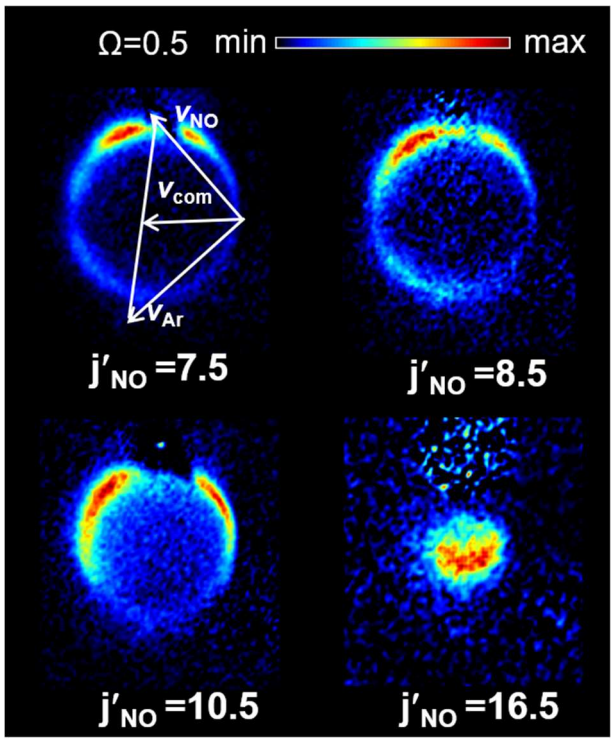

Fig. 4. Images of the inelastic scattering of NO with Ar into final rotational levels with quantum numbers j'_{NO} = 7.5, 8.5, 10.5 and 16.5 and f parity. A Newton diagram for the conditions of the experimental measurements is superimposed in the first panel.

3.2 Classical models for interpreting the physical origins of structures observed in DCSs

We are not aware of any prior reports of classical or quantum mechanical scattering calculations for the NO + CH_4 system with which to compare our experimental results. We therefore turn to simpler model treatments to guide our interpretation. The measurements show that the direction of the scattering changes from the forward to the backward hemisphere as the amount of angular momentum imparted to the NO product increases, and classical mechanics provides a qualitative explanation of this trend. Low rotational levels of NO can be populated by large impact parameter collisions at relatively long range, in glancing impacts that result in only a small deflection of the NO, and hence a small transfer of initial linear and orbital angular momenta into product rotational angular momentum. A higher degree of product rotational excitation implies a larger torque during the collision. This larger torque is generated by collisions with smaller impact parameters, and these more head-on collision geometries generally result in more backscattering.

Considering that methane is a spherical top molecule, it is possible that the inelastic scattering of NO with CH_4 can be directly compared to that of NO with Ar. Figure 5 depicts such a comparison of the extracted DCSs for the NO product rotational levels of j'_{NO} = 7.5, 8.5, 10.5, and 16.5 for the two systems. For j'_{NO} = 7.5 and 8.5, the DCSs of the NO + CH_4 system are peaked toward a lower scattering angle than those of the NO + Ar system. Moreover, there is only a single obvious broad maximum in the DCSs of the NO + CH_4 system, whereas one dominant and two minor peaks are seen for j'_{NO} = 7.5 from NO + Ar collisions. However, for j'_{NO} =10.5 and 16.5, the DCSs show reasonable agreement between the two systems. As is shown in supplementary Figure S8, rotational rainbow angles can be well predicted with a 2-dimensional hard ellipse model for the inelastic scattering of Ar with NO. This model, proposed by Bosanac *et al.*, ignores attractive forces between the two species and approximates the repulsive interaction by a hard ellipse.[52, 53] It is therefore reasonable to suppose that the same model can aid the interpretation of inelastic scattering data for NO collisions with CH_4, at least for population of higher final rotational levels of the product NO. Here, we approximate that the methane molecule behaves as a structureless atom without internal degree of freedom. For an atom-ellipse hard collision model, the rotational rainbow angle θ_r satisfies Equation (1):[28, 51, 52]

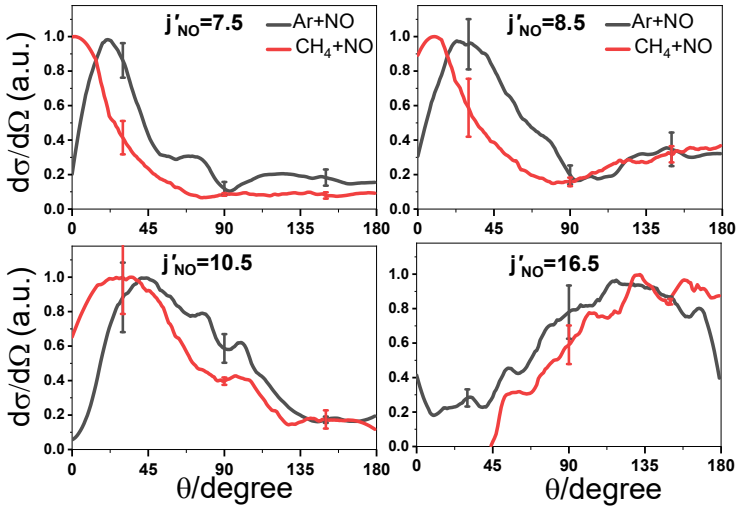

Fig. 5. A comparison of differential cross sections for NO scattering from Ar (black curves) and CH_4 (red curves) for four different final j'_{NO} rotational levels of f parity, as labelled in the panels.

$$\sin\left(\frac{\theta_r}{2}\right) = \frac{j_f}{2P_i b_{max}} \quad (1)$$

In this equation, j_f is the final rotational angular momentum, P_i is the incident momentum of the colliding atom, and $b_{max} = A - B$ is the difference between the major semi-axis A and the minor axis B of the ellipse, and is related to the anisotropy of the interaction potential. The rotational rainbow angles increase with increasing rotational angular momentum transfer, $\Delta j = j_f - j_i$ and under our experimental conditions the initial angular momentum j_i is small, so can be neglected. As is shown in Figure 6, by adjusting the anisotropy of the ellipse (i.e. b_{max}), the predicted rainbow angles can be made to match closely the rainbow angles observed experimentally for high j′ NO. As we move to lower j′ NO, the two-dimensional hard ellipse model increasingly fails to capture the observed angles, particularly for j′ NO = 7.5 and 8.5. We suspect this to be a consequence of increased sampling of the attractive part of the potential energy surface. The value of b_{max} used for this comparison is 0.34 Å, which nearly equals the average experimental value of b_{max} = 0.32 Å for the NO + Ar system.[38]

Images for j'_{NO} = 7.5 and 8.5 from NO collisions with CH_4 show strong scattering into the 0°-10° range which may arise from attractive forces between the collision partners. Although the role of attractive forces in rotational energy transfer has received less attention than collisions dominated mainly by repulsive forces, it is known that the existence of an attractive well in the PESs may give rise to an L-type rainbow. The occurrence of an L-type rainbow is manifested as an interference pattern at relatively small scattering angles.[54] The scattering angle is zero degrees for glory scattering, corresponding to an impact parameter for which the attractive and repulsive forces acting on the scattered particle balance perfectly.[44] As the impact parameter increases further, the attractive part of the potential is sampled more heavily than the repulsive part, giving rise to a non-zero but small scattering angle, which is the classical mechanism of an L-type rainbow.[55] Quantum mechanically, the L-type rainbow originates from partial waves with higher total angular momentum J than the glory partial wave, and therefore only occurs when these high partial waves contribute to the scattering cross-section. As these large-J partial waves cannot transfer sufficient energy to excite the NO to high rotational levels, L-type rainbows are particularly prominent for low Δj_{NO}

transitions.[41] The purely repulsive 2-dimensional hard ellipse model cannot account for the maxima observed at small forward scattering angles for these lower final j'_{NO} products, and we therefore propose that the strong scattering into the 0-10° range can be attributed to L-type rather than rotational rainbows.

Within an L-type rainbow model, the angle θ_L at which the L-type rainbow is expected for inelastic scattering of a rare gas atom with a diatomic molecule can be approximated by[30, 41]

$$\boldsymbol{\theta_L = 2\frac{\varepsilon}{E_{coll}}} \qquad (2)$$

where ε and E_{coll} are the average well depth of the PES and the collision energy, respectively. In contrast to the rotational rainbow, the L-type rainbow scattering only depends on the system and the collision energy, and not on the rotational excitation of the scattered molecule. Using the minimum (114.4 cm^{-1}) of the isotropic potential as the average well depth, the position of the L-type rainbows θ_L predicted by this model for NO + Ar scattering is 14° at a collision energy of 730 cm^{-1} for Ar + NO ($^2\Pi_{1/2}$, j=1/2) →Ar + NO ($^2\Pi_{1/2}$, j′=3/2, 5/2).[41] The average well depth of the PES for CH_4-NO van der Waals complexes is 95.5 cm^{-1},[56] hence the L-type rainbow angle θ_L calculated with equation (2) for the NO + CH_4 system is 15.6° under our experimental conditions. As is shown in Figure 6, this predicted rainbow angle is in reasonable agreement with the measured angles of 4° and 11° for NO in final rotational states of j'_{NO} =7.5 and j'_{NO}= 8.5, respectively. Although not quantitatively predictive, the two-dimensional hard ellipse model and the L-type model can offer qualitative and valuable insights into the origin of structures in the quantum-state resolved DCSs.

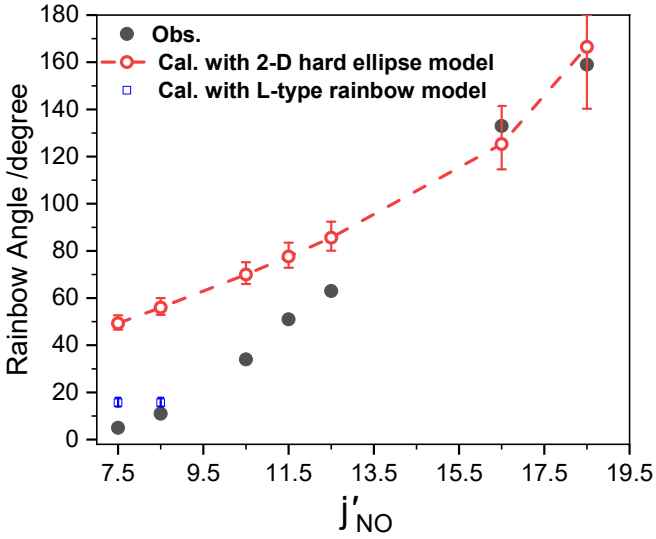

Fig. 6. The observed (solid black circles) and calculated (open red circles) dependence of rotational rainbow angles on final rotational level j'_{NO} for NO scattering from CH_4. Blue squares represent angles calculated with the L-type rainbow model. The error bars are obtained by taking the spread of collision energies into account.

3.3 Rotational excitation of CH_4 co-products

The analysis of experimental velocity-map images for the scattering of diatomic NO from a polyatomic molecule such as CH_4 is more complicated than the analysis of collisions of NO with rare gas atoms because of the possibility of change of the internal energies of both the NO and its molecular collision partner. However, the analysis of the images potentially provides rich information about pairwise correlations between the final rotational levels of the two molecules involved in collisions, in this case the (j'_{NO}, j'_{CH4}) correlation. Since both the NO and CH_4 molecules can undergo rotational excitation during the collision, the experimental image for a specific final rotational level of NO, which is state-selectively detected in the REMPI scheme, is a sum over the scattering for all the rotational states of co-product CH_4 populated in coincidence. Within the NO images, the rotational excitation is observed as a series of concentric rings, corresponding to the Newton spheres for the scattered CH_4 co-products in different final j'_{CH4} states, but overlapping because of the experimental resolution. The radial size of a NO image is proportional to the center-of-mass frame speed of the scattered NO. This radial size decreases with increasing j'_{CH4} according to the kinetic energy available to the NO molecule after partitioning the

initial collisional and internal energies into both NO and CH_4 post-collision rotational excitation (E_{rot}').

The total translational energy of the two products, $E_t = E_{coll} - \Delta E_{rot}$, is a function of both NO and CH_4 pre- and post-collision rotational energies because the change in the rotational energy from the collision, $\Delta E_{rot} = E_{rot}' - E_{rot}$, contains contributions from both NO and CH_4. The initial rotational energies of the NO and CH_4 molecules, E_{rot}, are those of the rotational levels of the NO and CH_4 molecules populated in the molecular beams. As described in section 2, about 90% of NO molecules are in $j_{NO} = 0.5$. Due to the expansion of neat CH_4 molecules to form the second molecular beam, the initial conditions of CH_4 molecules are not as well controlled: we estimate 31% of CH_4 molecules are in j_{CH4}=0, 56% in j_{CH4}=1 and 13% in j_{CH4}=2 based on work by Buck et al.[38] An ion image can be blurred by the spreads in the initial velocity and angular distributions of the two molecular beams, together with the distribution of populations of rotational levels of the CH_4 molecules, which together cause an overlap of the scattered NO Newton spheres, leading to a broad distribution of NO speeds from the image analysis. Comparison of the radial widths of features in NO images from scattering with Ar demonstrates that much of the broadening can be attributed to the rotational excitation of CH_4 co-products. The mean collision energy for the CH_4 + NO system is 700 cm^{-1} with a FWHM of the distribution of 80 cm^{-1}. Within the principles of energy and linear momentum conservations, the rotational energy of the co-product CH_4 is determined by:

$$E_{rot}(CH_4)' = E_{coll} - E_t' - E_{rot}(NO)' + E_{rot}(CH_4) + E_{rot}(NO) \quad (3)$$

with primes denoting product properties. Here, E_t' is the total translational kinetic energy of both scattered products, and other terms have been defined earlier. We consider E_{rot} for each species to be that of its most populated energy level, i.e. j_{NO}=0 and j_{CH4}=1

Since CH_4 is a spherical top with a rotational constant of 5.2412 cm^{-1},[57] the rotational energy levels of CH_4 can be estimated directly from a given product translational energy measurement. In Figure 7, we superimpose the CH_4 product rotational level assignments onto total translational energy distributions obtained for the scattered NO product rotational levels of j'_{NO} = 7.5, 11.5, 13.5, and

18.5. Total translational energy distributions are obtained by integrating over all CM-frame scattering angles. Because of the additional noise introduced by the FINA method, and similar overall profiles for the total translational energy distributions obtained from unreconstructed and reconstructed images, the total translational energy distributions obtained from the unreconstructed images are preferred for this analysis. The corresponding plots for j'_{NO} = 8.5, 10.5, 12.5, and 16.5 are given in Supplementary Figure S11. As mentioned previously, the ±80 cm^{-1} spread in collision energies places some uncertainty on the derivation of the rotational level j'_{CH4}. Hence, the rotational levels j'_{CH4} were estimated for the three cases of minimum (620 cm^{-1}), mean (700 cm^{-1}), and maximum (780 cm^{-1}) initial collision energies. Even using the maximum collision energy to estimate the rotational level assignments for CH_4, a small part of the measured high total translational energy distribution cannot be assigned. It is possible that CH_4 and NO molecules with higher pre-collision rotational energies, present because of imperfect cooling in the molecular beams, give rise to this higher energy component.

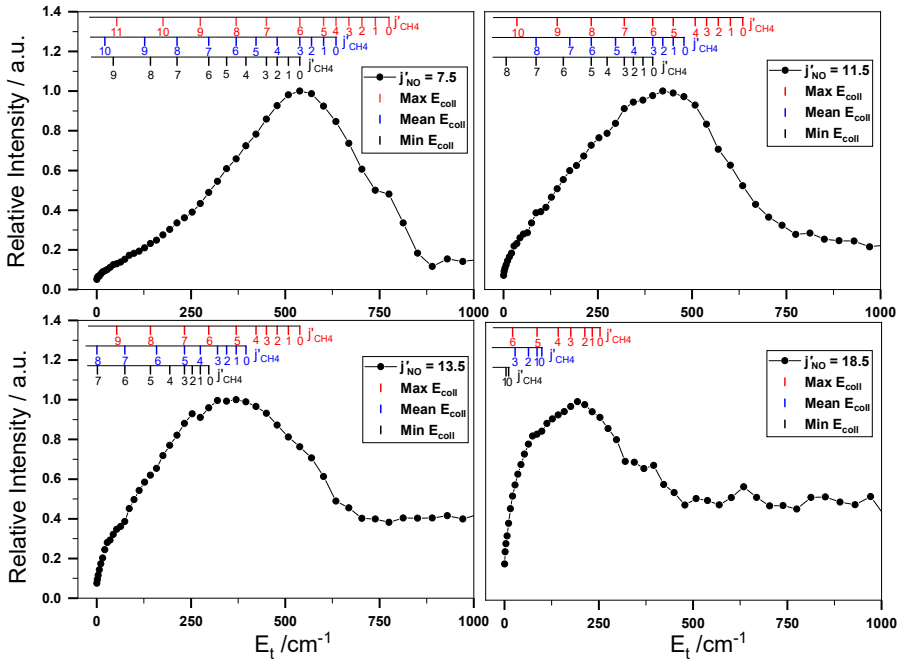

Fig. 7. Total translational energy distributions of the scattered NO + CH_4 collision products, obtained by integrating over all CM-frame scattering angles for j'_{NO} = 7.5, 11.5, 13.5, and 18.5. Using arguments of conservation of energy and linear momentum, the combs at the top of each panel represent the positions of co-product CH_4 rotational levels estimated with three different collision energies encompassing the experimental spread of 700 ± 80 cm^{-1}.

We further focus on the most probable rotational levels $j'_{CH4,}$ corresponding to the peaks in the total translational energy distributions, shown in Figure 7. The most probable j'_{CH4} values deduced using the mean (700 cm^{-1}) and maximum (780 cm^{-1}) initial collision energies are shown in the upper panel of Figure 8. It should be noted that at the minimum collision energy, the co-product CH_4 cannot be rotational excited according to energy constraint arguments. As the rotational excitation of the detected NO molecule increases, the overall trend of the most probable j'_{CH4} value decreases for j'_{NO} values from 7.5 to 18.5, but remains nearly constant in the j'_{NO} range from 8.5 to 13.5. This trend suggests that higher Δj_{NO} for the scattered NO correlates with lower Δj_{CH4} of the co-product CH_4, corresponding to a product-pair anti-correlation of rotational excitation in this bimolecular scattering. In other words, the warmer j'_{NO} is, the colder j'_{CH4} will be.

In Figure 8(a), the black and red dashed lines represent the maximum accessible rotational levels of CH_4 deduced by assuming that all the collision and initial internal energies are transferred into rotational energies of both scattered products. The maximum j'_{CH4} values shown by the dashed lines are consistently larger than the most probable j'_{CH4} values deduced for the same j'_{NO} values from the experiments. Therefore, this product-pair anti-correlation of rotational excitation is not driven by energy constraints. Figure 8(b) proposes a classical explanation for the observed trend of anti-correlation of rotational excitation of the NO and CH_4 products. Equal and opposite forces act on the atoms when two molecules approach most closely (see the lower panel of Figure 8), independent of whether the forces are attractive or repulsive. For collisions with large impact parameter, CH_4 molecules experience a large torque because the center-of-mass of the molecule is on the C atom, resulting in excitation of higher CH_4 rotational levels. The partner NO is forward scattered, and experiences lower rotational excitation than collisions at lower impact parameter which sample more of the repulsive potential. However, for these collisions with small impact parameter, smaller torques on the CH_4 molecules lead to low or no rotational excitation, whereas the partner NO is backward scattered and excited rotationally by the repulsive interaction. In other words, collisions at the central C-atom do not induce rotational excitation of CH_4, whereas collisions at a peripheral H-atom do. These arguments apparently conflict with reports of positively correlated product rotational excitations in diatomic-diatomic molecule inelastic collisions.[16-18, 58] However, the opposing correlations may arise from differences in the physical shapes of methane

(a spherical top) and linear molecules. Further theoretical work is required to provide a more quantitative understanding of the rotationally inelastic scattering dynamics of NO with CH_4, and in particular this rotational anti-correlation in the product pairs. Theoretical simulations are currently impeded by the lack of a global PES for the NO + CH_4 system and the complexity of the diatomic + polyatomic molecule scattering dynamics.

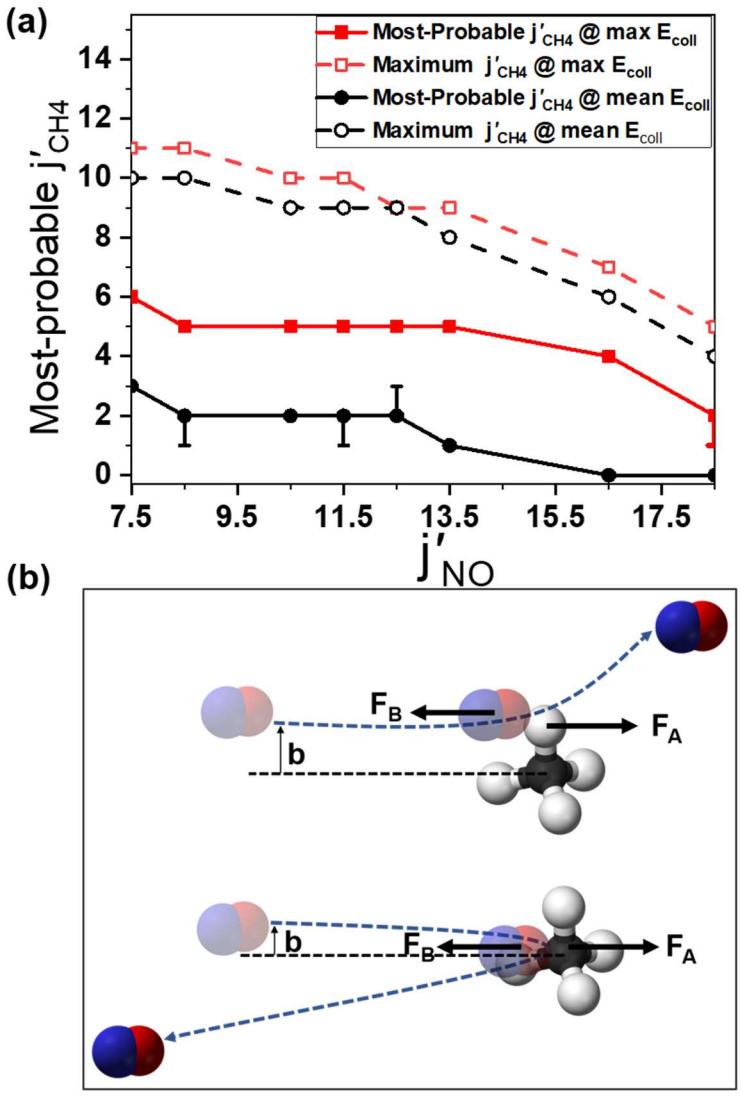

Fig. 8. Dependence of rotational excitation of the co-product CH_4 on the final rotational level of NO. (a) Most-probable j'_{CH4} values for each partner j'_{NO} deduced from analysis of the radial intensity dependence of scattered NO velocity-map images. The j'_{CH4} values were determined from the rotational level assignments corresponding to peaks in the translational energy distributions shown in Figure 7. The error bars are obtained by taking the uncertainty of peak position in the translational energy distributions into account. Dashed lines show the predictions for maximum rotational excitation accessible on energy conservation grounds. Black and red points and lines

correspond to data analysis using the mean (700 cm^{-1}) and maximum (780 cm^{-1}) experimental collision energies, respectively. (b) Schematic diagram for the mechanism of rotational excitation of the co-product CH_4. The NO and CH_4 molecules approach each other with different impact parameters b, and interact with repulsive forces F_A and F_B, generating different torques on the CH_4.

4. CONCLUSIONS

We report the observation of rotational and L-type rainbows in the rotationally inelastic scattering of NO with CH_4 at a collision energy of 700 ± 80 cm^{-1}. Although detailed comparison with scattering calculations on a global potential energy surface is not yet possible, classical models provide valuable insights for this inelastic scattering of the two molecular species. The measured NO quantum-state specific differential cross sections will provide a stringent test for the quality of future potential energy surfaces, and for any approximations of reduced dimensionality applied to quantum scattering calculations for the NO + CH_4 system. The high Δj_{NO} scattered products appear to be correlated with low Δj_{CH4} co-product CH_4 molecules, which indicates a product-pair anti-correlation of rotational excitation in this bimolecular scattering.

All experimental data are archived in the University of Bristol's Research Data Storage Facility (DOI: 10.5523/bris.2ggbg99gidvbn2ddlzfxk2fcit)

Supporting Information

Experimental methods. Density-to-flux transformation. Image reconstruction for partial slicing. Λ-doublet transitions. Rotational rainbows observed in the inelastic scattering of Ar + NO. Images for spin-orbit changing collisions of CH_4 with NO. Rotational excitation of CH_4 co-products. (PDF)

ACKNOWLEDGMENTS

We thank EPSRC for funding via Programme Grant EP/L005913/1. FJJC acknowledges award of EPSRC Doctoral Training Grant funding (EP/N509619/1).

REFERENCES

(1) Roueff, E.; Lique, F. Molecular Excitation in the Interstellar Medium: Recent Advances in

Collisional, Radiative, and Chemical Processes. *Chem. Rev.* **2013,** *113*, 8906-8938.

(2) Schiffman, A.; Chandler, D. W. Experimental Measurements of State-Resolved, Rotationally Inelastic Energy-Transfer. *Int. Rev. Phys. Chem.* **1995,** *14*, 371-420.

(3) Dagdigian, P. J. Theoretical Investigation of Collisional Energy Transfer in Polyatomic Intermediates. *Int. Rev. Phys. Chem.* **2013,** *32*, 229-265.

(4) Wade, E. A.; Thomas Lorenz, K.; Chandler, D. W.; Barr, J. W.; Barnes, G. L.; Cline, J. I. Ion Imaging Studies of Product Rotational Alignment in Collisions of NO with Ar. *Chem. Phys.* **2004,** *301*, 261-272.

(5) Kohguchi, H.; Suzuki, T.; Alexander, M. H. Fully State-Resolved Differential Cross Sections for the Inelastic Scattering of the Open-Shell NO Molecule by Ar. *Science* **2001,** *294*, 832-834.

(6) Brouard, M.; Chadwick, H.; Eyles, C. J.; Hornung, B.; Nichols, B.; Aoiz, F. J.; Jambrina, P. G.; Stolte, S. Rotational Alignment Effects in NO(X) + Ar Inelastic Collisions: an Experimental Study. *J. Chem. Phys.* **2013,** *138*, 104310-104323.

(7) Lorenz, K. T.; Chandler, D. W.; Barr, J. W.; Chen, W.; Barnes, G. L.; Cline, J. I. Direct Measurement of the Preferred Sense of NO Rotation after Collision with Argon. *Science* **2001,** *293*, 2063-2066.

(8) Sarma, G.; Marinakis, S.; ter Meulen, J. J.; Parker, D. H.; McKendrick, K. G. Inelastic Scattering of Hydroxyl Radicals with Helium and Argon by Velocity-Map Imaging. *Nat. Chem.* **2012,** *4*, 985-989.

(9) Chadwick, H.; Nichols, B.; Gordon, S. D.; Hornung, B.; Squires, E.; Brouard, M.; Klos, J.; Alexander, M. H.; Aoiz, F. J.; Stolte, S. Inelastic Scattering of NO by Kr: Rotational Polarization over a Rainbow. *J. Phys. Chem. Lett.* **2014,** *5*, 3296-3301.

(10) Vogels, S. N.; Onvlee, J.; Chefdeville, S.; van der Avoird, A.; Groenenboom, G. C.; van de Meerakker, S. Y. Imaging Resonances in Low-Energy NO-He Inelastic Collisions. *Science* **2015,** *350*, 787-790.

(11) Tkáč, O.; Ma, Q.; Stei, M.; Orr-Ewing, A. J.; Dagdigian, P. J. Rotationally Inelastic Scattering of Methyl Radicals with Ar and N_2. *J. Chem. Phys.* **2015,** *142*, 014306-014316.

(12) Tkáč, O.; Saha, A. K.; Loreau, J.; Ma, Q.; Dagdigian, P. J.; Parker, D. H.; van der Avoird, A.; Orr-Ewing, A. J. Rotationally Inelastic Scattering of ND_3 with H_2 as a Probe of the Intermolecular Potential Energy Surface. *Mol. Phys.* **2015,** *113*, 3925-3933.

(13) Gao, Z.; Loreau, J.; van der Avoird, A.; van de Meerakker, S. Y. T. Direct Observation of Product-Pair Correlations in Rotationally Inelastic Collisions of ND_3 with D_2. *Phys. Chem. Chem. Phys.* **2019,** *21*, 14033-14041.

(14) Vogels, S. N.; Karman, T.; Klos, J.; Besemer, M.; Onvlee, J.; van der Avoird, A.; Groenenboom, G. C.; van de Meerakker, S. Y. T. Scattering Resonances in Bimolecular Collisions Between NO Radicals and H_2 Challenge the Theoretical Gold Standard. *Nat. Chem.* **2018,** *10*, 435-440.

(15) Gao, Z.; Vogels, S. N.; Besemer, M.; Karman, T.; Groenenboom, G. C.; van der Avoird, A.; van de Meerakker, S. Y. T. State-to-State Differential Cross Sections for Inelastic Collisions of NO Radicals with para-H_2 and ortho-D_2. *J. Phys. Chem. A* **2017,** *121*, 7446-7454.

(16) de Jongh, T.; Karman, T.; Vogels, S. N.; Besemer, M.; Onvlee, J.; Suits, A. G.; Thompson, J. O. F.; Groenenboom, G. C.; van der Avoird, A.; van de Meerakker, S. Y. T. Imaging Diffraction Oscillations for Inelastic Collisions of NO Radicals with He and D_2. *J. Chem. Phys.* **2017,** *147*, 013918-013926.

(17) Gao, Z.; Karman, T.; Vogels, S. N.; Besemer, M.; van der Avoird, A.; Groenenboom, G. C.; van de Meerakker, S. Y. T. Observation of Correlated Excitations in Bimolecular Collisions. *Nat. Chem.* **2018,** *10*, 469-473.

(18) Gao, Z.; Karman, T.; Tang, G.; van der Avoird, A.; Groenenboom, G. C.; van de Meerakker, S. Y.

T. Correlated Energy Transfer in Rotationally and Spin-Orbit Inelastic Collisions of NO($X^2\Pi_{1/2}$, j = 1/2f) with $O_2(X^3\Sigma_g^-)$. *Phys. Chem. Chem. Phys.* **2018,** *20*, 12444-12453.

(19) Karman, T.; Besemer, M.; van der Avoird, A.; Groenenboom, G. C. Diabatic States, Nonadiabatic Coupling, and the Counterpoise Procedure for Weakly Interacting Open-Shell Molecules. *J. Chem. phys.* **2018,** *148*, 094105-09419.

(20) Buck, U.; Huisken, F.; Schleusener, J.; Schaefer, J. State Resolved Rotational Excitation in HD+D_2 Collisions. I. Angular Dependence of 0→1 Transitions. *J. Chem. Phys.* **1981,** *74*, 535-544.

(21) Buck, U.; Huisken, F.; Schleusener, J. Diffraction Oscillations in Rotationally Inelastic Differential Cross-Sections - Hd+D_2. *J. Chem. Phys.* **1978,** *68*, 5654-5655.

(22) Bacon, J. A.; Giese, C. F.; Gentry, W. R. State-to-State Differential Cross Sections for Rotationally Inelastic Collisions of NO($^2\Pi_{1/2}$, j⩽2.5) with CO($^1\Sigma^+$) and $O_2(^3\Sigma_g^-)$ at a kinetic energy of 442 cm^{-1}. *J. Chem. Phys.* **1998,** *108*, 3127-3133.

(23) Vonk, M. T.; Bacon, J. A.; Giese, C. F.; Gentry, W. R. Differential Cross Sections for Rotationally Inelastic Collisions of NO($^2\Pi_{1/2}$, j'⩽2.5) with NO(2Π1/2, j'⩽2.5) at a kinetic energy of 442 cm^{-1}. *J. Chem. Phys.* **1997,** *106*, 1353-1358.

(24) Wade, E. A.; Lorenz, K. T.; Springfield, J. L.; Chandler, D. W. Collisions of HCl with rare gas and molecular colliders. *J. Phys. Chem. A* **2003,** *107*, 4976-4981.

(25) Tkáč, O.; Orr-Ewing, A. J.; Dagdigian, P. J.; Alexander, M. H.; Onvlee, J.; van der Avoird, A. Collision Dynamics of Symmetric Top Molecules: a Comparison of the Rotationally Inelastic Scattering of CD_3 and ND_3 with He. *J. Chem. Phys.* **2014,** *140*, 134308-134318 .

(26) Tkáč, O.; Sage, A. G.; Greaves, S. J.; Orr-Ewing, A. J.; Dagdigian, P. J.; Ma, Q. L.; Alexander, M. H. Rotationally Inelastic Scattering of CD_3 and CH_3 with He: Comparison of Velocity Map-Imaging Data with Quantum Scattering Calculations. *Chem. Sci.* **2013,** *4*, 4199-4211.

(27) Schepper, W.; Ross, U.; Beck, D. Anisotropy of the Repulsive Intermolecular Potential from Rotationally Inelastic Scattering. *Z. Phys. A* **1979,** *290*, 131-141.

(28) Sarma, G.; Saha, A. K.; Bishwakarma, C. K.; Scheidsbach, R.; Yang, C. H.; Parker, D.; Wiesenfeld, L.; Buck, U.; Mavridis, L.; Marinakis, S. Collision Energy Dependence of State-to-State Differential Cross Sections for Rotationally Inelastic Scattering of H_2O by He. *Phys. Chem. Chem. Phys.* **2017,** *19*, 4678-4687.

(29) Levine. R. D.; Bernstein R. B. *Molecular Reaction Dynamics and Chemical Reactivity*. Oxford University Press: New York, 1987.

(30) Yang, M.; Watts, R. O. The Anisotropic Potential Energy Surfaces of H_2, N_2, and Ar with C_2H_2 from Total Differential Scattering Experiments. *J. Chem. Phys.* **1994,** *100*, 3582-3593.

(31) Eyles, C. J.; Brouard, M.; Yang, C. H.; Klos, J.; Aoiz, F. J.; Gijsbertsen, A.; Wiskerke, A. E.; Stolte, S. Interference Structures in the Differential Cross-Sections for Inelastic Scattering of NO by Ar. *Nat. Chem.* **2011,** *3*, 597-602.

(32) Pan, H.; Liu, K. Observation of a Reactive Rainbow in F + CH_3D → CH_2D(v = 0) + HF(v = 3)? *J. Phys. Chem. A* **2016,** *120*, 6712-6718.

(33) Bowman, J. M. Rotational Rainbows in Inelastic Atom-Molecule Differential Cross-Sections. *Chem. Phys. Lett.* **1979,** *62*, 309-311.

(34) Schinke, R.; Korsch, H. J.; Poppe, D. Rainbows in Rotationally Inelastic-Scattering - a Comparative-Study of Different Model Potential Surfaces and Dynamical Approximations. *J. Chem. Phys.* **1982,** *77*, 6005-6020.

(35) Aoiz, F. J.; Verdasco, J. E.; Brouard, M.; Klos, J.; Marinakis, S.; Stolte, S. Inelastic Scattering of He

atoms and NO($X^2\Pi$) molecules: the Role of Parity on the Differential Cross Section. *J. Phys. Chem. A* **2009,** *113*, 14636-14649.

(36) Eyles, C. J.; Brouard, M.; Chadwick, H.; Aoiz, F. J.; Klos, J.; Gijsbertsen, A.; Zhang, X.; Stolte, S. The Effect of Parity Conservation on the Spin-Orbit Conserving and Spin-Orbit Changing Differential Cross Sections for the Inelastic Scattering of NO(X) by Ar. *Phys. Chem. Chem. Phys.* **2012,** *14*, 5420-5439.

(37) Gijsbertsen, A.; Linnartz, H.; Stolte, S. Parity-Dependent Rotational Rainbows in D_2-NO and He-NO Differential Collision Cross Sections. *J. Chem. Phys.* **2006,** *125*, 133112-133122.

(38) Bontuyan, L. S.; Suits, A. G.; Houston, P. L.; Whitaker, B. J. State-Resolved Differential Cross Sections for Crossed-Beam Argon-Nitric Oxide Inelastic Scattering by Direct Ion Imaging. *J. Phys. Chem.* **1993,** *97*, 6342-6350.

(39) Klos, J.; Aoiz, F. J.; Menendez, M.; Brouard, M.; Chadwick, H.; Eyles, C. J. Ab Initio Studies of the Interaction Potential for the Xe-NO($X^2\Pi$) Van Der Waals Complex: Bound States and Fully Quantum and Quasi-Classical Scattering. *J. Chem. Phys.* **2012,** *137*, 014312-014326.

(40) Aoiz, F. J.; Verdasco, J. E.; Herrero, V. J.; Rabanos, V. S.; Alexander, M. A. Attractive and Repulsive Interactions in the Inelastic Scattering of NO by Ar: a Comparison between Classical Trajectory and Close-Coupling Quantum Mechanical Results. *J. Chem. Phys.* **2003,** *119*, 5860-5866.

(41) Onvlee, J.; Vogels, S. N.; van der Avoird, A. D.; Groenenboom, G. C.; van de Meerakker, S. Y. T. Resolving Rainbows with Superimposed Diffraction Oscillations in NO plus Rare Gas Scattering: Experiment and Theory. *New. J. Phys.* **2015,** *17*, 055019-055035.

(42) Western, C. *PGOPHER: A Program for Simulating Rotational, Vibrational and Electronic Spectra*, University of Bristol.

(43) Thompson, J. O. F.; Amarasinghe, C.; Foley, C. D.; Suits, A. G., Finite Slice Analysis (FINA) — A General Reconstruction Method for Velocity Mapped and Time-Sliced Ion Imaging. *J. Chem. Phys.* **2017,** *147*, 013913-013927.

(44) *Tutorials in Molecular Reaction Dynamics*; Brouard M., Vallance C., Royal Society of Chemistry: Cambridge, United Kingdom, 2010.

(45) Buck, U.; Kohlhase, A.; Secrest, D.; Phillips, T.; Scoles, G.; Grein, F. Rotationally Inelastic-Scattering and Potential Calculations for Ne + CH_4. *Mol. Phys.* **1985,** *55*, 1233-1253.

(46) Wang, F. Y.; Liu, K. P. Imaging the Effects of Bend-Excitation in the F + $CD_4(v_b=0,1) \rightarrow DF(v)$ + $CD3(v_2=1,2)$ Reactions. *J. Phys. Chem. A* **2013,** *117*, 8536-8544.

(47) Lin, J. J.; Zhou, J.; Shiu, W.; Liu, K. Application of Time-Sliced Ion Velocity Imaging to Crossed Molecular Beam Experiments. *Rev. Sci. Instrum.* **2003,** *74*, 2495-2500.

(48) Yonekura, N.; Gebauer, C.; Kohguchi, H.; Suzuki, T., A Crossed Molecular Beam Apparatus Using High-Resolution Ion Imaging. *Rev. Sci. Instrum.* **1999,** *70*, 3265-3270.

(49) Komissarov, A. V.; Minitti, M. P.; Suits, A. G.; Hall, G. E., Correlated Product Distributions from Ketene Dissociation Measured by DC Sliced Ion Imaging. *J. Chem. Phys.* **2006,** *124*, 014303-014315.

(50) Brouard, M.; Chadwick, H.; Eyles, C. J.; Hornung, B.; Nichols, B.; Scott, J. M.; Aoiz, F. J.; Klos, J.; Stolte, S.; Zhang, X., the Fully Quantum State-Resolved Inelastic Scattering of NO(X) plus Ne: Experiment and Theory. *Mol. Phys.* **2013,** *111*, 1759-1771.

(51) Westley, M. S.; Lorenz, K. T.; Chandler, D. W.; Houston, P. L. Differential Cross Sections for Rotationally Inelastic Scattering of NO from He and D_2. *J. Chem. Phys.* **2001,** *114*, 2669-2680.

(52) Bosanac, S. Two-Dimensional Model of Rotationally Inelastic Collisions. *Phys. Rev. A* **1980,** *22*,

2617-2622.
(53) Bosanac, S.; Buck, U. Rotational Rainbow Scattering from an Off-Center Rigid Shell-Model. *Chem. Phys. Lett.* **1981,** *81*, 315-319.
(54) Kłos, J.; Aoiz, F. J.; Menéndez, M.; Brouard, M.; Chadwick, H.; Eyles, C. J. Ab Initio Studies of the Interaction Potential for the Xe–NO(X $^2\Pi$) Van Der Waals Complex: Bound States and Fully Quantum and Quasi-Classical Scattering. *J. Chem. Phys.* **2012,** *137*, 014312-014326.
(55) Eyles, C. J.; Brouard, M.; Chadwick, H.; Aoiz, F. J.; Kłos, J.; Gijsbertsen, A.; Zhang, X.; Stolte, S. the Effect of Parity Conservation on the Spin–Orbit Conserving and Spin–Orbit Changing Differential Cross Sections for the Inelastic Scattering of NO(X) by Ar. *Phys. Chem. Chem. Phys.* **2012,** *14*, 5420-5439.
(56) Crespo-Otero, R.; Suardiaz, R.; Montero, L. A.; Vega, J. M. G. d. l. Potential Energy Surfaces and Jahn-Teller Effect on CH_4···NO Complexes. *J. Chem. Phys.* **2007,** *127*, 104305-104312.
(57) Herzberg, G., *Molecular spectra and molecular structure. Vol.3: Electronic spectra and electronic structure of polyatomic molecules*. Van Nostrand: New York, 1966.
(58) Brouard, M.; Gordon, S. D. S.; Nichols, B.; Squires, E.; Walpole, V.; Aoiz, F. J.; Stolte, S. Angular Distributions for the Inelastic Scattering of NO($X^2\Pi$) with $O_2(X^3\Sigma_g^-)$. *J. Chem. Phys.* **2017,** *146*, 204304-204316.

TOC Graphic